European Journal of Medicinal Chemistry 214 (2021) 113204

Contents lists available at ScienceDirect

European Journal of Medicinal Chemistry

journal homepage: http://www.elsevier.com/locate/ejmech

Identification of novel potent HIV-1 inhibitors by exploiting the tolerant regions of the NNRTIs binding pocket

Yanying Sun [a, c], Dongwei Kang [a, d, *], Feng Da [a, c], Tao Zhang [a, c], Pei Li [a], Baodan Zhang [a], Erik De Clercq [b], Christophe Pannecouque [b], Peng Zhan [a, c, **], Xinyong Liu [a, c, ***]

[a] Department of Medicinal Chemistry, Key Laboratory of Chemical Biology (Ministry of Education), School of Pharmaceutical Sciences, Cheeloo College of Medicine, Shandong University, 44 West Culture Road, 250012 Jinan, Shandong, PR China
[b] Rega Institute for Medical Research, Laboratory of Virology and Chemotherapy, K.U. Leuven, Herestraat 49 Postbus 1043 (09.A097), B-3000 Leuven, Belgium
[c] China-Belgium Collaborative Research Center for Innovative Antiviral Drugs of Shandong Province, 44 West Culture Road, 250012 Jinan, Shandong, PR China
[d] Suzhou Research Institute, Shandong University, Room522, Building H of NUSP, NO.388 Ruoshui Road, SIP, Suzhou, 215123 Jiangsu, PR China

ARTICLE INFO

Article history:
Received 22 August 2020
Received in revised form
30 November 2020
Accepted 12 January 2021
Available online 24 January 2021

Keywords:
HIV-1
DAPY
NNRTIs
NNIBP
Tolerant regions

ABSTRACT

With our previously identified potent NNRTIs **25a** and **HBS-11c** as leads, series of novel thiophene[3,2-*d*]pyrimidine and thiophene[2,3-*d*]pyrimidine derivatives were designed *via* molecular hybridization strategy. All the target compounds were evaluated for their anti-HIV-1 activity and cytotoxicity in MT-4 cells. Compounds **16a1** and **16b1** turned out to be the most potent inhibitors against WT and mutant HIV-1 strains (L100I, K103N, and E138K), with EC_{50} values ranging from 0.007 μM to 0.043 μM. Gratifyingly, **16b1** exhibited significantly reduced cytotoxicity (CC_{50} > 217.5 μM) and improved water solubility (S = 49.3 μg/mL at pH 7.0) compared to the lead 25a (S < 1 μg/mL at pH 7.0, CC_{50} = 2.30 μM). Moreover, molecular docking was also conducted to rationalize the structure-activity relationships of these novel derivatives and to understand their key interactions with the binding pocket.

1. Introduction

Human immunodeficiency virus (HIV) could enter the host cell and eventually lead to significant weakening of the host immune system, which was identified as the causative agent for the acquired immune deficiency syndrome (AIDS) [1,2]. HIV-1 reverse transcriptase (RT), an RNA-dependent DNA polymerase that uses single-stranded RNA templates to synthesize double-stranded viral DNA, is a validated important target in the discovery and development of novel anti-HIV drugs with the advantage of providing well characterized biochemical mechanisms and abundant structural information [3,4]. Amongst the HIV-1 RT inhibitors, non-nucleoside reverse transcriptase inhibitors (NNRTIs) have achieved significant attraction due to their remarkable antiviral activity, excellent specificity and reduced toxicity in antiretroviral therapy [5–7]. Up to now, there are six NNRTIs approved by the U.S. Food and Drug Administration (FDA), including the first generation nevirapine (NVP), delavirdine (DLV), efavirenz (EFV), the second generation etravirine (ETR), rilpivirine (RPV), and doravirine (DOR) [7,8]. However, drug resistance remains to be a severe problem with the first- and second-generation HIV-1 NNRTIs. K103N and Y181C have limited the clinical use of the first-generation NNRTIs NVP and EFV [9]. ETR and RPV are members of the diarylpyrimidine (DAPY) family (Fig. 1), which could effectively inhibit most RT-resistant mutations caused by the first-generation NNRTIs, but they generally failed to suppress the most refractory mutations E138K, while

* Corresponding author. Department of Medicinal Chemistry, Key Laboratory of Chemical Biology (Ministry of Education), School of Pharmaceutical Sciences, Cheeloo College of Medicine, Shandong University, 44 West Culture Road, 250012 Jinan, Shandong, PR China.
** Corresponding author. Department of Medicinal Chemistry, Key Laboratory of Chemical Biology (Ministry of Education), School of Pharmaceutical Sciences, Cheeloo College of Medicine, Shandong University, 44 West Culture Road, 250012 Jinan, Shandong, PR China.
*** Corresponding author. Department of Medicinal Chemistry, Key Laboratory of Chemical Biology (Ministry of Education), School of Pharmaceutical Sciences, Cheeloo College of Medicine, Shandong University, 44 West Culture Road, 250012 Jinan, Shandong, PR China.
E-mail addresses: kangdongwei@sdu.edu.cn (D. Kang), zhanpeng1982@163.com (P. Zhan), xinyongl@sdu.edu.cn (X. Liu).

https://doi.org/10.1016/j.ejmech.2021.113204
0223-5234/

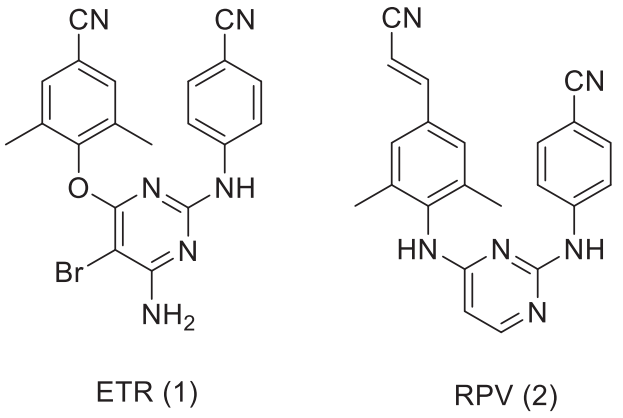

Fig. 1. Chemical structures of diarylpyrimidine (DAPY)-based HIV-1 NNRTIs approved by U.S. FDA.

V106A and F227L are the two most prevalent mutations selected by DOR [10–12]. Additionally, the patients treated with second-generation NNRTIs were frequently reported with hypersensitivity reactions and other adverse effects [13,14]. Therefore, the development of new NNRTIs with greater potency, improved drug-resistance profiles, and less toxicity is urgently needed [14–17].

With ETR and RPV as leads, our previous efforts have led to the development of some novel and potent HIV-1 NNRTIs [18–23], including piperidine-substituted thiophene[3,2-*d*]pyrimidine derivative **3** (**25a**) as potent HIV-1 NNRTI (Fig. 2) [24]. The "four-point pharmacophore" model (including the hydrophobic channel, hydrogen bonding domain, tolerant region I, and tolerant region II) of diarylpyrimidine (DAPY) derivatives in the NNRTI binding pocket (NNIBP) was also confirmed by the co-crystal structures of HIV-1 wild-type (WT) RT in complex with **25a** for the first time [25]. However, **25a** suffered from higher cytotoxicity (CC_{50} = 2.30 μM) and poor water solubility (<1 μg/mL at pH 7.0). Interestingly, another research in our lab culminated in the identification of potent NNRTIs **4** (**HBS-11c**) with improved water solubility (= 30.92 μg/mL at pH 7.0) by exploiting the tolerant region I of NNIBP, indicating that the solvent-exposed regions could be regarded as favorable sites for substantial modifications of existing NNRTIs without serious loss of activity [14].

Encouraged by these interesting findings and in attempt to yield HIV-1 NNRTIs with more potent activity, lower cytotoxicity and favorable solubility, series of novel thiophene[3,2-*d*]pyrimidine and thiophene[2,3-*d*]pyrimidine derivatives were designed based on the co-crystal structure of **25a**/WT RT and molecular hybridization strategy (Fig. 2). The target compounds incorporated the common left wing of **25a** and **HBS-11c**, right wing of **HBS-11c** and central core of **25a** according to the DAPY's "four-point phaemacophore" model. Meanwhile, 1-phenylpiperazine and 1-phenylpiperidin-3-amine motifs were introduced to replace the 1-benzylpiperazine motif of the lead to further investigate the structure-activity relationship (SAR) of the tolerant region I. These newly synthesized compounds were evaluated for their anti-HIV-1 activities and cytotoxicity in MT-4 cells. In addition, molecular docking studies were undertaken to guide further investigation.

2. Results and discussion

2.1. Chemistry

The synthetic protocols for the novel designed compounds are illustrated in Schemes 1-2. First, the treatment of 1-fluoro-4-

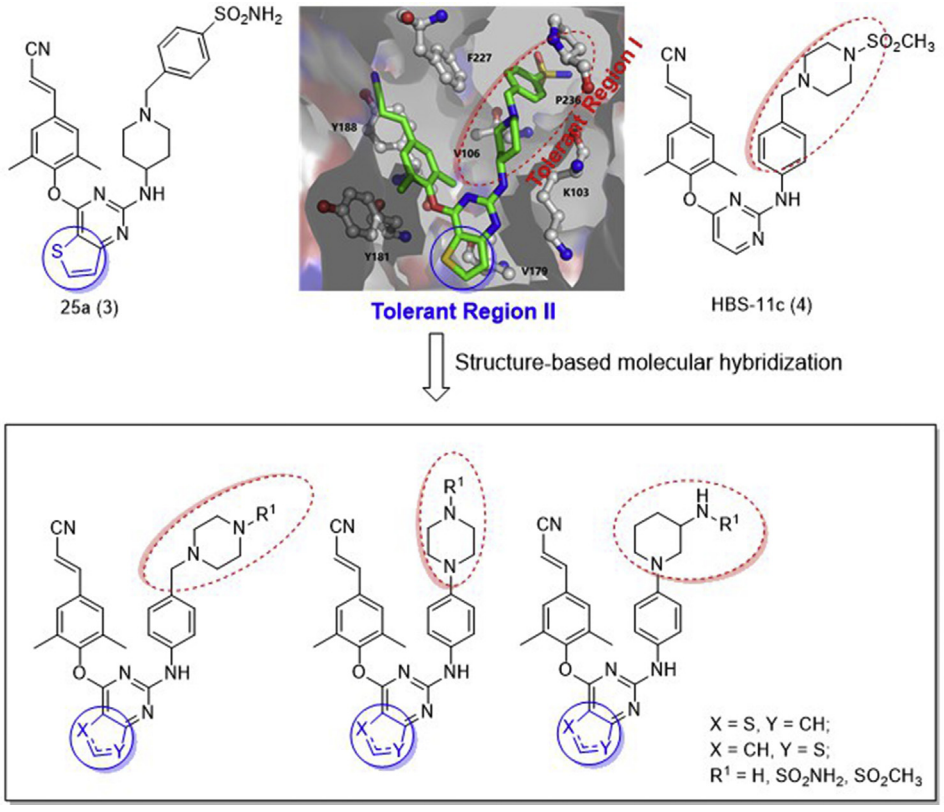

Fig. 2. Design of novel NNRTIs by exploiting the tolerant regions of NNIBP.

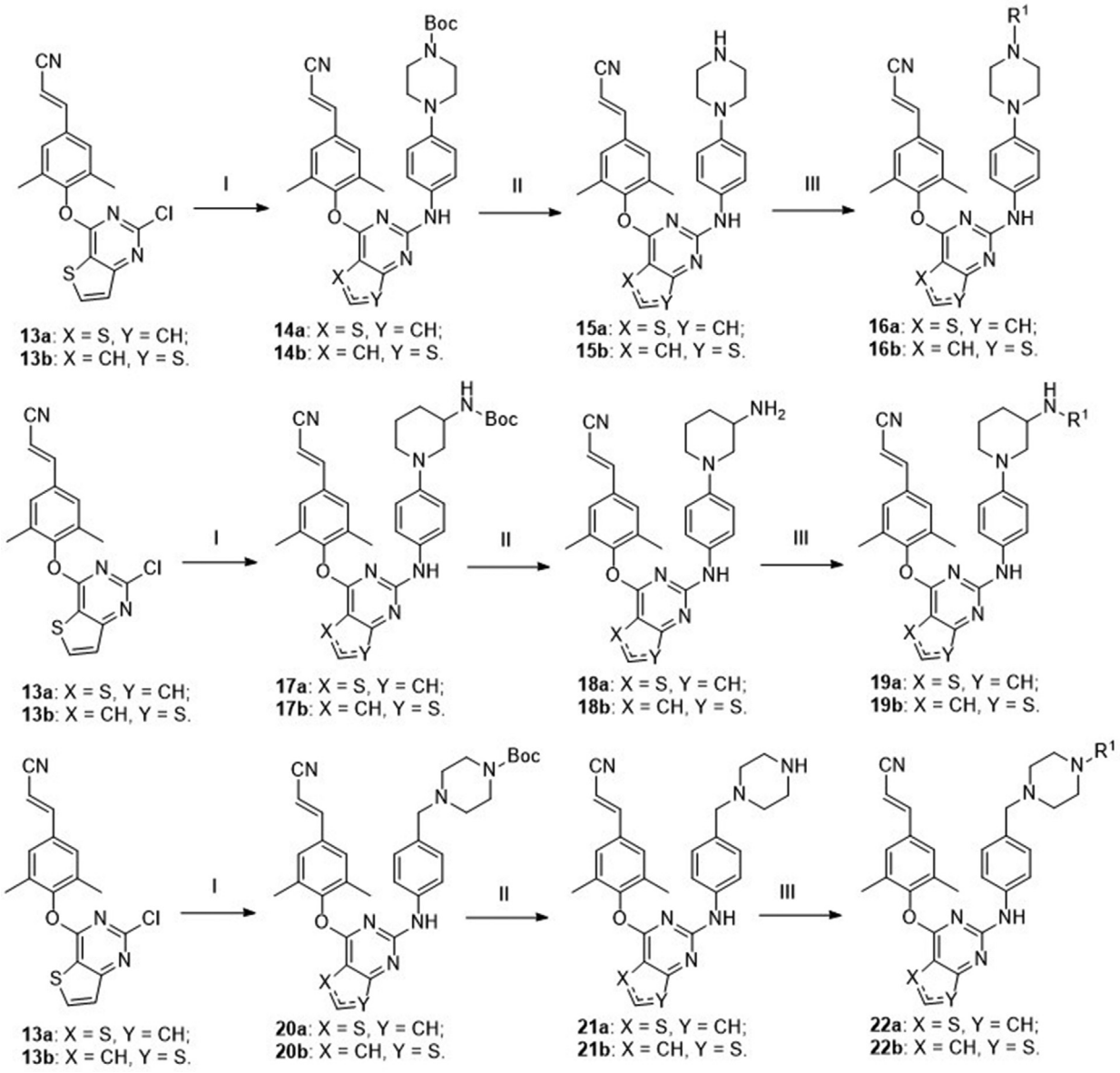

Scheme 1. Synthesis of the intermediates 7, 9 and 12[a].

nitrobenzene (**5**) with *tert*-butyl piperazine-1-carboxylate and *tert*-butyl piperidin-3-ylcarbamate gave intermediates **6** and **8**, respectively, which provided intermediates **7** and **9** via reduction in the presence of Pd/C and H_2 in excellent yields. 4-Nitrobenzyl bromide (**10**) reacted with *tert*-butyl piperazine-1-carboxylate *via* a nucleophilic substitution reaction afforded compound **11**, which by reduction gave the intermediate **12** (Scheme 1).

[a]Reagents and conditions: i) DMSO, 120 °C; ii) Pd/C, H_2, MeOH, r.t.; iii) *tert*-butyl piperazine-1-carboxylate, K_2CO_3, DMF, r.t.

[a]Reagents and conditions: i) BINAP, $Pd_2(dba)_3$, Cs_2CO_3, 1,4-dioxane, 90 °C, N_2; ii) TFA, DCM, r.t.; iii) CH_3SO_2Cl or NH_2SO_2Cl, Et_3N, DCM, r.t.

As described in Scheme 2, the previously prepared intermediates **13a** and **13b** in our lab were selected as starting materials [22,24], which were treated with the obtained intermediates **7**, **9** and **12** to prepare **14a-b, 17a**−**b** and **20a**−**b** *via* Buchwald−Hartwig reaction. Subsequent removal of the tert-butyloxycarbonyl (Boc) protecting group using trifluoroacetic acid (TFA) afforded free amines **15a-b**, **18a**−**b** and **21a**−**b**, and the resulting free amines were treated with methanesulfonyl chloride or sulfamoyl chloride in the presence of triethylamine to yield the target compounds.

2.2. In vitro anti-HIV-1 activity and cytotoxicity

For all novel chemical entities, antiviral activity, expressed as EC_{50} (anti-HIV-1 potency), CC_{50} (cytotoxicity), and SI (selectivity index, CC_{50}/EC_{50} ratio), was measured against WT HIV-1 (IIIB) and a panel of NNRTIs-resistant single and double mutant strains, including L100I, K103N, Y181C, Y188L, E138K, F227L + V106A, and RES056 (K103N + Y181C). The approved drugs NVP, EFV, ETR and RPV were selected as controls.

As shown in Table 1, in the case of the HIV-1 IIIB, nine compounds (**15b**, **16a1**, **16b1**, **16b2**, **19a1**, **19a2**, **19b1**, **22a1** and **22b1**) exhibited higher potency with EC_{50} values ranging from 0.007 to 0.126 μM, which are superior to that of the reference drug NVP (EC_{50} = 0.150 μM). Among them, **16a1** (EC_{50} = 0.007 μM) and **16b1** (EC_{50} = 0.008 μM) turned out to be the most potent inhibitors,

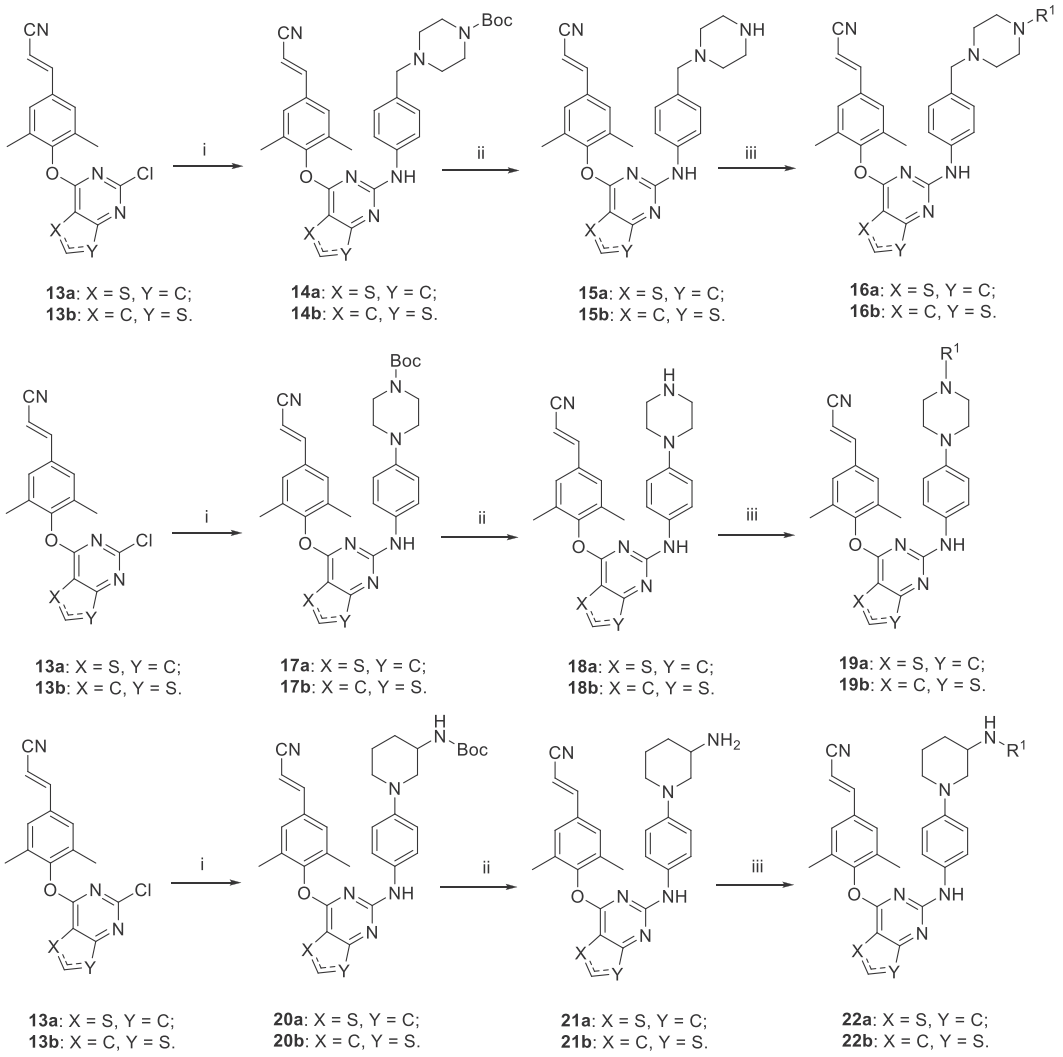

Scheme 2. Synthesis of the target compounds[a].

being comparable to that of the reference drug ETR (EC_{50} = 0.004 μM) and RPV (EC_{50} = 0.001 μM). Gratifyingly, **16b1** (CC_{50} > 217.5 μM, SI > 26923) exhibited much lower cytotoxicity compared to RPV (CC_{50} = 3.98 μM, SI = 3989), which contribute to its higher selectivity index value toward HIV-1 IIIB.

The preliminary SAR indicated that the thiophene[3,2-*d*]pyrimidine and thiophene[2,3-*d*]pyrimidine center rings have little effect on the anti-HIV-1 activity of the compounds. However, the scaffold substitution of the right wing has great influence on their potency. Compounds of subseries **16** and subseries **19** showed better activity than those of subseries **22**, i.e., **16a1** (EC_{50} = 0.007 μM) > **19a1** (EC_{50} = 0.027 μM) > **22a1** (EC_{50} = 0.059 μM); **16b1** (EC_{50} = 0.008 μM) > **19b1** (EC_{50} = 0.028 μM) > **22b1** (EC_{50} = 0.126 μM); **16b2** (EC_{50} = 0.036 μM) > **19b2** (EC_{50} = 0.172 μM) > **22b2** (EC_{50} = 1.431 μM). These results suggested that the 1-benzylpiperazine motif could contribute more to the activity than that of the 1-phenylpiperazine and 1-phenylpiperidin-3-amine motif. Next, we turned our attention to the SAR of the R^1 substituent of the right ring. Replacement the H atom of compounds **15a-b**, **18a-b** and **21a-b** with SO_2CH_3 group has an uncertain effect on the activity of the compound; i.e., **16a2** and **22b2** showed weaker activity, while the activity of **16b2** and **22a2** increased slightly compared to those of **15a-b** and **21a-b**. A SO_2NH_2 substituent in this region seems essential for high antiviral potency; **16a1**, **16b1**, and **19b1** with SO_2NH_2 substituent turned out to be more effective inhibitors with EC_{50} values of 0.007–0.028 μM. Moreover, the compounds had higher cytotoxicity when R^1 was H (**15a-b**, **18a-b** and **21a-b**, CC_{50} = 3.817 − 5.732 μM), while most compounds with SO_2NH_2 and SO_2CH_3 substituent in R^1 position afforded advantageous features of decreased cytotoxicity with high therapeutic index, with the exception of **16a2** (CC_{50} = 20.70 μM) and **19a2** (CC_{50} = 11.54 μM).

Furthermore, the target compounds **16a1-2**, **16b1-2**, **19a1-2**, **19b1-2**, **22a1-2**, and **22b1-2** were evaluated for their activity against a panel of NNRTI-resistance mutations, including L100I, K103N, Y181C, Y188L, E138K, F227L + V106A, and RES056. As displayed in Table 2 and Table S1, all the target inhibitors exhibited moderate to excellent potency against single-mutant strains and double-mutant strain F227L + V106A, but some inhibitors lost their activity against the double-mutant strain RES056. Especially, **16a1** and **16b1** turned out to be the most potent inhibitors among all the tested compounds. As for mutant HIV-1 strain L100I, **16a1** and **16b1** yielded EC_{50} values of 0.043 μM and 0.015 μM, respectively, which were comparable to that of EFV (EC_{50} = 0.031 μM). In the case of K103N mutant HIV-1 strain, both **16a1** (EC_{50} = 0.007 μM,

Table 1
Activity and cytotoxicity against HIV-1 IIIB strain.

Compds	R[1]	EC_{50} (μM)[a] (IIIB)	CC_{50} (μM)[b]	SI[c]
15a	H	0.216 ± 0.052	3.970 ± 1.113	18
15b	H	0.042 ± 0.008	4.030 ± 0.883	94
16a1	SO_2NH_2	0.007 ± 0.002	145.3 ± 51.92	18979
16a2	SO_2CH_3	0.391 ± 0.240	20.70 ± 4.010	53
16b1	SO_2NH_2	0.008 ± 0.002	>217.5	>26923
16b2	SO_2CH_3	0.036 ± 0.012	131.1 ± 2.028	3557
18a	H	0.387 ± 0.125	5.732 ± 0.215	15
18b	H	0.584 ± 0.146	4.737 ± 0.512	8
19a1	SO_2NH_2	0.027 ± 0.009	>222.9	>8310
19a2	SO_2CH_3	0.027 ± 0.008	11.54 ± 1.984	428
19b1	SO_2NH_2	0.028 ± 0.012	>222.9	>7790
19b2	SO_2CH_3	0.172 ± 0.045	>222.5	>1295
21a	H	0.815 ± 0.259	3.817 ± 1.166	5
21b	H	0.461 ± 0.178	4.613 ± 0.611	10
22a1	SO_2NH_2	0.059 ± 0.029	>217.5	>3632
22a2	SO_2CH_3	0.450 ± 0.211	>217.1	>434
22b1	SO_2NH_2	0.126 ± 0.045	>217.5	>1726
22b2	SO_2CH_3	1.431 ± 0.307	111.8 ± 15.11	78
NVP	–	0.150 ± 0.036	>15.02	>100
EFV	–	0.028 ± 0.0007	>6.335	>2268
ETR	–	0.004 ± 0.0007	>4.594	>1105
RPV[d]	–	0.001 ± 0.0003	3.98	3989

[a] EC_{50}: Concentration of compound required to achieve 50% protection of MT-4 cell cultures against HIV-1-induced cytopathic effect, as determined by the MTT method.
[b] CC_{50}: Concentration required to reduce the viability of mock-infected cell cultures by 50%, as determined by the MTT method.
[c] SI: the ratio of CC_{50}/EC_{50}.
[d] Used for comparison. Data were reported in Ref. 22.

SI = 202134) and **16b1** (EC_{50} = 0.007 μM, SI > 28409) exhibited single-digit nanomolar activity and higher SI values, being far more potent than NVP (EC_{50} = 3.992 μM, SI > 4) and EFV (EC_{50} = 0.071 μM, SI > 89), and comparable to ETR (EC_{50} = 0.003 μM, SI > 1417) and RPV (EC_{50} = 0.002 μM, SI = 3045). Morevoer, **16b2**, **19a1**, **19a2** and **19b1** also showed comparable antiviral activity (EC_{50} = 0.021 − 0.056 μM) to EFV. In the case of Y181C and E138K, **16b1** (EC_{50} = 0.045 and 0.025 μM, SI > 4836 and 8636, respectively) exhibited the most active potency, while **16a1** exhibited the greatest potency to Y188L and F227L + V106A (EC_{50} = 0.544 and 0.175 μM, SI = 267 and 830, respectively). However, both of them exhibited significantly reduced inhibition of RES056 mutant strain (EC_{50} = 1.911 and 1.384 μM, respectively) compared to other mutant strains.

2.3. Inhibition of HIV-1 RT

Next, all prepared compounds were assayed *in vitro* for their ability to inhibit recombinant WT to validate their binding target. Similarly, the FDA-approved drug NVP, EFV, ETR and RPV were selected as the controls. The results of this evaluation are summarized in Table 3.

The results demonstrated that all compounds (IC_{50} = 0.103 − 4.790 μM) displayed lower binding-affinity to WT HIV-1 RT compared to that of EFV (IC_{50} = 0.008 μM), ETR (IC_{50} = 0.012 μM) and RPV (IC_{50} = 0.015 μM). Furthermore, the data clearly showed that the antiviral activities of these compounds were inconsistent with their enzyme inhibitory potencies. As observed in most NNRTI series, the differences between cell activity and enzyme activity are considered to be caused by template-specific variation in the relationship between HIV-RT-RNA binding affinity and polymerase processivity [12]. Although the most potent inhibitors 16a1 (IC_{50} = 0.961 μM) and 16b1 (IC_{50} = 0.295 μM) exhibited much lower activity than that of ETR, their activity was comparable to that of NVP (IC_{50} = 0.575 μM), which confirmed that those newly designed compounds could inhibit the activity of HIV-1 RT and acted as typical HIV-1 NNRTIs.

Furthermore, the preliminary SAR of enzyme activity was concluded. Generally, subseries **22** exhibited the highest IC_{50} values

Table 3
Inhibitory activity against WT HIV-1 RT.

Compds	IC_{50} (μM)[a]	Compds	IC_{50} (μM)[a]
15a	0.707 ± 0.230	19b2	0.239 ± 0.006
15b	0.151 ± 0.020	21a	1.582 ± 0.065
16a1	0.961 ± 0.121	21b	0.956 ± 0.131
16a2	0.139 ± 0.038	22a1	2.411 ± 0.389
16b1	0.299 ± 0.047	22a2	0.775 ± 0.040
16b2	0.103 ± 0.020	22b1	4.790 ± 0.005
18a	0.945 ± 0.184	22b2	1.015 ± 0.030
18b	0.849 ± 0.111	NVP	0.575 ± 0.177
19a1	0.214 ± 0.044	EFV	0.008 ± 0.002
19a2	0.211 ± 0.021	ETR[b]	0.012 ± 0.002
19b1	0.713 ± 0.045	RPV[b]	0.015 ± 0.001

[a] IC_{50}: inhibitory concentration of test compounds required to inhibit biotin deoxyuridine triphosphate (biotin-dUTP) incorporation into WT HIV-1 RT by 50%.
[b] The data were obtained from the same laboratory with the same method (Prof. Erik De Clercq, Rega Institute for Medical Research, KU Leuven, Belgium). Data were reported in Ref. 22.

Table 2
Anti-HIV-1 activity against HIV-1 mutant strains.

Compds	EC_{50} (μM)[a]						
	L100I	K103 N	Y181C	Y188L	E138K	F227L + V106A	RES056
16a1	0.043 ± 0.006	0.007 ± 0.002	0.154 ± 0.021	0.544 ± 0.185	0.026 ± 0.016	0.175 ± 0.071	1.911 ± 0.791
16a2	1.560 ± 0.868	0.356 ± 0.076	5.636 ± 0.485	>20.70	0.983 ± 0.157	2.198 ± 0.316	>20.70
16b1	0.015 ± 0.008	0.007 ± 0.001	0.045 ± 0.006	0.877 ± 0.162	0.025 ± 0.012	0.369 ± 0.237	1.384 ± 0.323
16b2	0.387 ± 0.187	0.054 ± 0.018	1.270 ± 0.239	9.414 ± 1.192	0.162 ± 0.023	1.638 ± 0.851	18.78 ± 3.517
19a1	0.767 ± 0.318	0.021 ± 0.002	2.249 ± 0.703	23.11 ± 17.73	0.043 ± 0.015	0.203 ± 0.111	>222.9
19a2	0.938 ± 0.224	0.056 ± 0.019	4.531 ± 1.526	5.114 ± 1.368	0.088 ± 0.038	0.285 ± 0.065	>11.54
19b1	0.409 ± 0.100	0.031 ± 0.004	1.360 ± 0.274	10.14 ± 4.023	0.050 ± 0.014	0.331 ± 0.150	195.6 ± 13.06
19b2	3.322 ± 1.902	0.219 ± 0.099	42.73 ± 19.03	68.43 ± 17.40	0.405 ± 0.119	1.952 ± 0.274	175.4 ± 31.02
22a1	1.660 ± 0.575	0.102 ± 0.022	3.640 ± 0.444	6.754 ± 1.750	0.123 ± 0.075	0.381 ± 0.082	>217.5
22a2	6.823 ± 3.870	0.461 ± 0.176	43.40 ± 8.064	150.0 ± 30.48	1.285 ± 0.070	16.78 ± 6.917	>217.1
22b1	2.329 ± 0.571	0.450 ± 0.160	7.532 ± 1.462	88.20 ± 18.47	0.621 ± 0.244	3.639 ± 1.661	>217.5
22b2	8.519 ± 4.286	1.358 ± 0.524	14.01 ± 0.410	16.17 ± 1.591	4.272 ± 0.778	13.78 ± 1.554	16.53 ± 2.884
NVP	0.622 ± 0.276	3.922 ± 0.675	5.053 ± 0.921	9.074 ± 2.406	0.168 ± 0.098	8.041 ± 3.532	>15.02
EFV	0.031 ± 0.008	0.071 ± 0.020	0.005 ± 0.001	0.260 ± 0.117	0.005 ± 0.001	0.380 ± 0.247	0.335 ± 0.149
ETR	0.008 ± 0.002	0.003 ± 0.0008	0.015 ± 0.004	0.018 ± 0.006	0.009 ± 0.004	0.025 ± 0.016	0.060 ± 0.034
RPV[b]	0.002 ± 0.000	0.002 ± 0.0004	0.005 ± 0.0005	0.079 ± 0.0008	0.006 ± 0.0001	0.081 ± 0.021	0.010 ± 0.008

[a] EC_{50}: Concentration of compound required to achieve 50% protection of MT-4 cell cultures against HIV-1-induced cytopathic effect, as determined by the MTT method.
[b] Used for comparison. Data were reported in Ref. 22.

than that of subseries **16** and subseries **19**, indicating that 1-phenylpiperidin-3-amine motif located in the right wing would result in a decreased inhibitory activity compared to that of 1-phenylpiperazine and 1-benzylpiperazine motif. Additionally, the compounds containing SO_2CH_3 substituent on R^1 position offered higher RT inhibitory activities in each subseries than those with SO_2NH_2 substituent, exemplified by these pairwise comparisons: **16a1** vs **16a2**, **16b1** vs **16b2**, **19a1** vs **19a2**, **19b1** vs **19b2**, **22a1** vs **22a2**, and **22b1** vs **22b2**.

2.4. Water solubility measurement

Moreover, the most potent inhibitors **16a1** and **16b1** were evaluated for their water solubility at different pH values (2.0, 7.0, and 7.4) [14]. As depicted in Table 4, both compounds possessed desirable solubility at different pH values. Especially, **16a1** and **16b1** exhibited significantly enhanced solubility at pH 7.0 (S = 49.7 and 49.3 μg/mL, respectively) and pH 7.4 (S = 39.5 and 38.9 μg/mL, respectively), which were much greater than that of **25a** and ETR.

2.5. Molecular modeling analysis

To fully understand the binding mode of the newly designed compounds to the NNIBP, the molecular docking for the selected compounds **15a**, **16a1**, **19a1** and **22a1** was carried out using the software SurflexeDock SYBYL-X 2.0 by following a previously reported methodology. Co-crystal structure of WT HIV-1 RT (PDB code: 6c0n) and RES056 HIV-1 RT (PDB code: 6c0r) were used as the input structures for docking calculations [25]. Docking results were visualized with PyMOL and illustrated in Figs. 3 and 4.

As shown in Fig. 3, compounds **15a**, **16a1**, and **19a1** adopted a horseshoe conformation in the NNIBP, as is typically found for most NNRTIs (Fig. 3A) in the DAPY family. Especially, the most potent compound **16a1** (Fig. 3B) exhibited a series of well-known interactions with NNIBP: (i) the surface-positioned sulfonamide group arched into the tolerant region I and formed double-hydrogen bonding with the backbone carbonyl oxygen and nitrogen of Val106; (ii) the N atom of the thiophene[3,2-*d*]pyrimidine and the amine group linking the central core and the piperidine ring interacts with the main-chain backbone of Lys101, developing double hydrogen bond observed in numerous of NNRTIs/RT complexes, which is important for maintaining effective antiviral activity; (iii) the left wing projected into the tunnel lined by Tyr181, Tyr188, Phe227, and Trp229, forming π-π interactions with these residues. However, the change of the right wing of these inhibitors result in the key water-mediated hydrogen bonding with the backbone Lys103 disappeared, which responsible for their reduced activity toward HIV-1 IIIB.

Additionally, compared with **16a1**, the 1-phenylpiperazine structure of the right wing of **19a1** (Fig. 3C) causes the sulfonamide group to deviate from Val106 and resulted in the disappearance of the hydrogen bond; while **15a** (Fig. 3E) cannot develop the hydrogen-bonding interaction with Val106. Although compound **22a1** (Fig. 3D) with 1-phenylpiperidin-3-amine scaffold in the right wing could still form the critical hydrogen bond with Val104, the classical horseshoe conformation was changed, and the shift of the left wing causing decreased π-π interactions with Tyr181 and Tyr188, may account for its reduced antiviral potency.

In the binding mode of **16a1** and **19a1** with HIV-1 RES056 RT (Fig. 4), the Lys103 to Asn103 substitution in RT brings the dramatic changes of the NNIBP, and results in the disappearance of the hydrogen-bonding interaction disappeared between Lys101 and thiophene[2,3-*d*]pyrimidine compared to that of the lead **25a** (Fig. 4A); the Tyr181 to Cys181 substitution leads to the greatly reduced π−π stacking interactions between the left wing of inhibitors and NNIBP. The above two reasons lead to the compounds significant decreased activity against RES056. Compared to **19a1** (Figs. 4C), **16a1** (Fig. 4B)is able to establish hydrogen bonding with the main chain of Lys104 by varying the position of the piperazine-linked sulfonamide group; the cyan group in the left wing could develop additional hydrogen-bonding interactions with Lys223, which account for its better resistance profiles than **19a1**.

Table 4
The solubility of compounds **16a1** and **16b1**.

Compds	Water solubility (μg/mL)		
	pH = 2.0	pH = 7.0	pH = 7.4
16a1	73.1	49.7	39.5
16b1	64.9	49.3	38.9
25a	84.7	5.26	<1
ETR	127	<1	<1

3. Conclusion

To discover novel HIV-1 NNRTIs with more potent activity, lower cytotoxicity and favorable solubility, series of novel thiophene[3,2-*d*]pyrimidine and thiophene[2,3-*d*]pyrimidine derivatives were designed applying by four-point pharmacophore model and fragment-based molecular hybridization strategy. We report the synthesis and biological evaluation of these novel analogues. The antiviral activity results demonstrated that compounds **16a1** and **16b1** afforded the most potent activity, exhibiting nanomole potency against WT, L100I, K103N, and E138K, with EC_{50} values ranging from 0.007 μM to 0.043 μM. Moreover, **16b1** also turned out to be a 0.045 μM inhibitor of Y181C. Furthermore, **16b1** exhibited significantly improved water solubility (S = 49.3 μg/mL at pH 7.0) and reduced cytotoxicity (CC_{50} > 217.5 μM) compared to the lead **25a** (S < 1 μg/mL at pH 7.0, CC_{50} = 2.30 μM). In addition, the molecular docking results indicated that double hydrogen bonding with the backbone of Lys101 and Val106, π-π interactions with Tyr181 and Tyr188 are responsible for the promising in vitro activity of these novel compounds.

4. Experimental section

4.1. Chemistry

All reactions were routinely monitored by thin layer chromatography on Silica Gel GF254 (Merck). Flash column chromatography was performed on columns packed with Silica Gel (200−300 mesh, Qingdao Haiyang Chemical Company). Solvents were purified and dried by standard methods. All melting points were determined on a micro melting point apparatus (RY-1G, Tianjin TianGuang Optical Instruments). ^{1}H NMR and ^{13}C NMR spectra were recorded in DMSO-d_6 on a Bruker AV-400 spectrometer with tetramethylsilane (TMS) as the internal standard. Chemical shifts are reported in δ values (ppm) from TMS and coupling constants are given in hertz; signals are abbreviated as s (singlet), d (doublet), and m (multiplet). The mass spectra were measured in A G1313A Standard LC Autosampler (Agilent).

4.1.1. Preparation of tert-butyl 4-(4-aminophenyl)piperazine-1-carboxylate (7)

A mixture of 1-fluoro-4-nitrobenzene (**5**, 1.41 g, 10 mmol) and *tert*-butyl piperazine-1-carboxylate (1.86 g, 10 mmol) in DMSO (20 mL) was heated at 120 °C overnight. Then the solution was cooled to ambient temperature and 100 mL of ice water was added. Stirring was continued for another 15 min, and the resulting

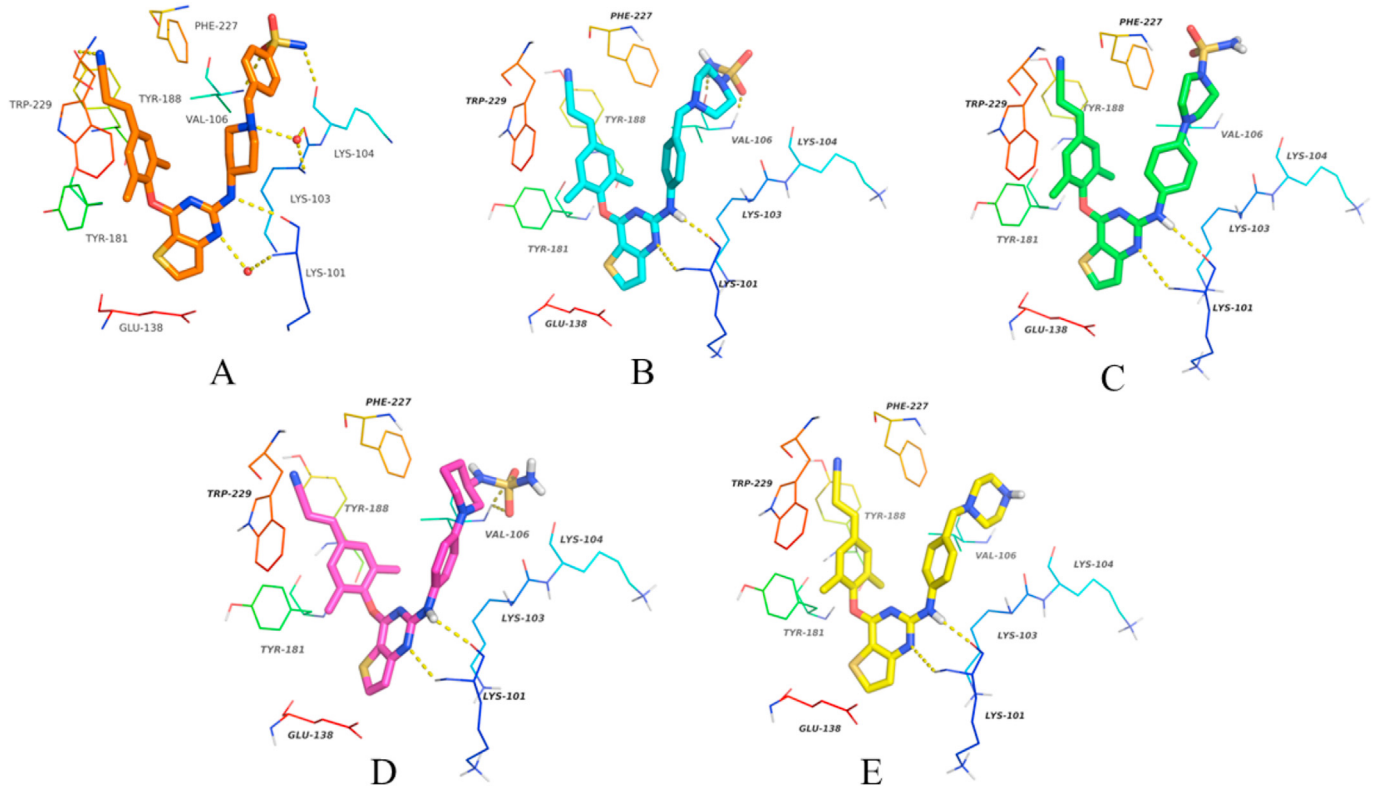

Fig. 3. The cocrystal structure of **25a**/WT RT (A) and predicted binding modes of **16a1** (B), **19a1** (C), **22a1** (D) and **15a** (E) with the HIV-1 WT RT (PDB code: 6c0n). The hydrogen bonds are indicated with yellow dashed lines. Nonpolar hydrogen atoms are not shown for clarity.

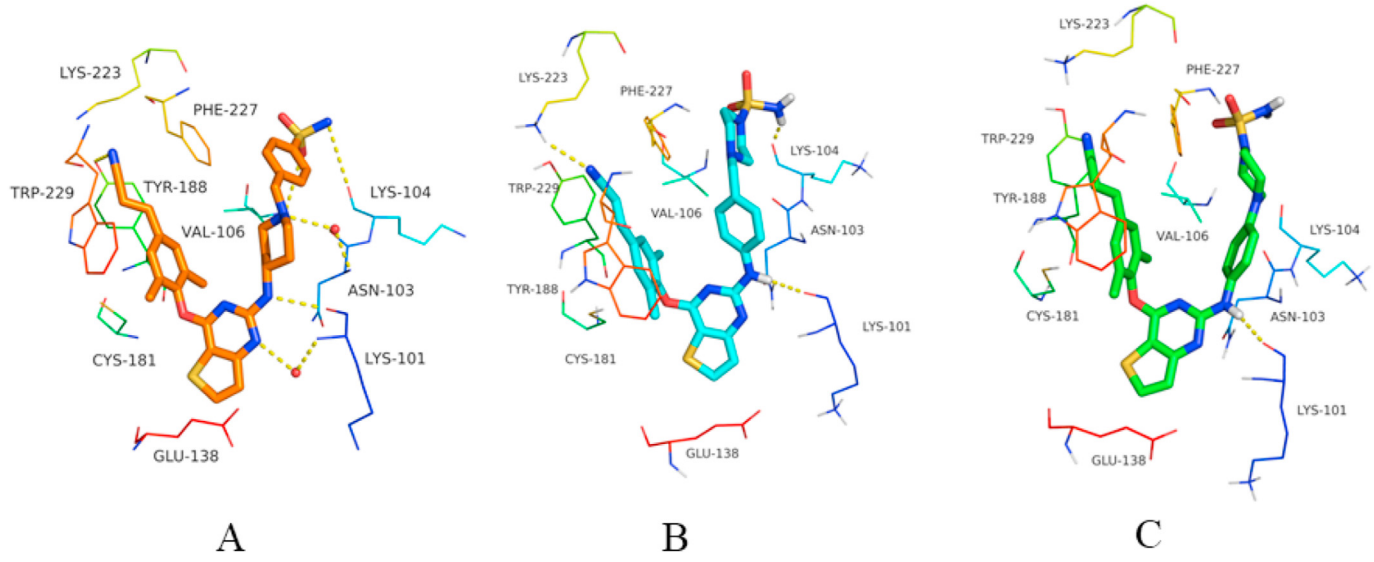

Fig. 4. The cocrystal structure of **25a**/RES056RT (A) and predicted binding modes of **16a1** (B) and **19a1** (C) with the HIV-1 RES056 RT (PDB code: 6c0r). The hydrogen bonds are indicated with yellow dashed lines. Nonpolar hydrogen atoms are not shown for clarity.

precipitate was collected by filtration and dried to give crude intermediate **6**, which was used directly in the next step without further purification. To a solution of intermediate **6** (0.31 g, 1.0 mmol) in methanol (15 mL) was added 10% palladium on carbon (wet) (0.21 g, 0.10 mmol), and the resulting mixture was stirred under an atmosphere of hydrogen gas overnight. The reaction mixture was filtered through a plug of Celite and the filtrate was evaporated under reduced pressure to afford intermediate **7** as white solid. The crude intermediate **7** was used in the next step without further purification. ESI-MS: *m/z* 278.5 $[M+1]^+$. $C_{15}H_{23}N_3O_2$ (277.18).

4.1.2. Preparation of tert-butyl (1-(4-aminophenyl)piperidin-3-yl) carbamate (9)

The synthetic procedure was similar to that of **7**, but the starting material was 1-fluoro-4-nitrobenzene (**5**, 1.41 g, 10 mmol) and *tert*-

butyl piperidin-3-ylcarbamate (2.00 g, 10 mmol). ESI-MS: *m/z* 292.4 $[M+1]^+$. $C_{16}H_{25}N_3O_2$ (291.19).

4.1.3. Preparation of tert-butyl 4-(4-aminobenzyl)piperazine-1-carboxylate (12)

A mixture of 1-(bromomethyl)-4-nitrobenzene (**10**, 2.14 g, 10 mmol), *tert*-butyl piperazine-1-carboxylate (1.86 g, 10 mmol) and K_2CO_3 (1.52 g, 11 mmol) in DMF (40 mL) was stirred at ambient temperature for 5 h (monitored by TLC); then to the solution was added 200 mL of ice water and it was stirred for another 15 min. The resulting precipitate was collected by filtration and dried to give crude intermediate **11** as yellow solid, which was used directly in the next step without further purification. To a solution of intermediate **11** (0.32 g, 1.0 mmol) in methanol (15 mL) was added 10% palladium on carbon (wet) (0.21 g, 0.10 mmol), and the resulting mixture was stirred under an atmosphere of hydrogen gas overnight. The reaction mixture was filtered through a plug of Celite and the filtrate was evaporated under reduced pressure to afford intermediate **12** as a white solid. ESI-MS: *m/z* 292.7 $[M+1]^+$. $C_{16}H_{25}N_3O_2$ (291.19).

4.1.4. General procedure for the preparation of intermediates 15a-b, 18a-b and 21a–b

In a schlenk-type flask, the starting materials **13a** (or **13b**, 0.34 g, 1.0 mmol) and intermediate **7** (or **9**, **12**, 1.2 mmol) were dissolved in dry dioxane (20 mL), and then $Pd_2(dba)_3$ (0.09 g, 0.1 mmol), BINAP (0.06 g, 0.1 mmol) and Cs_2CO_3 (0.97 g, 3.0 mmol) were added. The resulting mixture was stirred at 120 °C under the atmosphere of nitrogen for 10 h. Then the solvent was evaporated under reduced pressure, and the residue was purified by flash column chromatography to give intermediates **14a-b**, **17a-b** and **20a**–**b**. Then the intermediates were dissolved in DCM (5 mL), which was followed by addition of TFA (10 mmol) at room temperature. The solution was stirred for another 6 h (monitored by TLC). The mixed solution was alkalized to pH 9 with saturated $NaHCO_3$ and extracted with DCM (3 × 10 mL). Then organic phase was dried over anhydrous Na_2SO_4, filtered and purified by flash column chromatography. Recrystallized from ethyl acetate/petroleum ether to give intermediates **15a-b**, **18a-b** and **21a**–**b**, respectively.

4.1.5. (E)-3-(3,5-dimethyl-4-((2-((4-(piperazin-1-ylmethyl)phenyl)amino)thieno[3,2-d]pyrimidin-4-yl)oxy)phenyl)acrylonitrile (15a)

Recrystallized from EA/PE as a yellow solid, 67% yield, mp: 163–164 °C. ^{1}H NMR (400 MHz, DMSO-d_6) δ 9.51 (s, 1H, NH), 7.73 (d, J = 16.7 Hz, 1H, ArCH =), 7.51–7.43 (m, 2H, C_2, C_6-Ph''-H), 7.40 (s, 2H, C_2, C_6-Ph' –H), 7.18 (d, J = 4.2 Hz, 1H, C_6-thiophene-H), 7.04 (d, J = 4.5 Hz, 1H, C_7-thiophene-H), 7.02–6.96 (m, 2H, C_3, C_5-Ph''-H), 6.72 (d, J = 16.7 Hz, 1H, = CHCN), 3.00 (d, J = 3.7 Hz, 2H, CH_2), 2.52–2.50 (m, 4H), 2.48–2.42 (m, 4H), 2.12 (s, 6H), 1.09–1.05 (m, 1H, NH). ^{13}C NMR (100 MHz, DMSO-d_6) δ 164.84, 158.26, 140.11, 137.55, 131.91, 131.57, 129.49, 128.26, 124.32, 118.63, 107.20, 61.75, 50.67, 50.13, 46.16, 43.97, 29.04, 16.60, 16.52. ESI-MS: *m/z* 497.7 $[M + 1]^+$. $C_{28}H_{28}N_6OS$ (496.20).

4.1.6. (E)-3-(3,5-dimethyl-4-((2-((4-(piperazin-1-ylmethyl)phenyl)amino)thieno[2,3-d]pyrimidin-4-yl)oxy)phenyl)acrylonitrile (15b)

Recrystallized from EA/PE as a white solid, 54% yield, mp: 162–164 °C. ^{1}H NMR (400 MHz, DMSO-d_6) δ 9.65 (s, 1H, NH), 7.71 (dt, J = 6.0, 4.1 Hz, 2H, C_2, C_6-Ph''-H), 7.56 (s, 2H, C_2, C_6-Ph'-H), 7.48 (dt, J = 6.0, 4.1 Hz, 2H, C_3, C_5-Ph''-H), 7.37 (d, J = 16.5 Hz, 1H, ArCH =), 6.98 (d, J = 5.1 Hz, 1H, C_6-thiophene-H), 6.72 (d, J = 5.1 Hz, 1H, C_5-thiophene-H), 6.50 (d, J = 16.7 Hz, 1H, = CHCN), 3.39 (s, 2H, N–CH_2), 3.08–3.05 (m, 4H), 2.57–2.40 (m, 4H), 2.13 (s, 6H), 1.34 (s, 1H, NH). ^{13}C NMR (100 MHz, DMSO-d_6) δ 171.87, 162.69, 156.77, 152.26, 150.56, 139.73, 132.00, 131.82, 129.50, 128.74, 121.31, 119.42, 118.77, 96.88, 61.61, 50.67, 49.42, 43.53, 29.04, 16.58. ESI-MS: *m/z* 497.7 $[M + 1]^+$. $C_{28}H_{28}N_6OS$ (496.20).

4.1.7. (E)-3-(3,5-dimethyl-4-((2-((4-(piperazin-1-yl)phenyl)amino)thieno[2,3-d]pyrimidin-4-yl)oxy)phenyl)acrylonitrile (18b)

Recrystallized from EA/PE as a white solid, 67% yield, mp: 171–172 °C. ^{1}H NMR (400 MHz, DMSO-d_6) δ 9.45 (s, 1H, NH), 7.71 (d, J = 11.9 Hz, 1H, C_6-thiophene-H), 7.70 (d, J = 15.7 Hz, 1H, ArCH =), 7.57 (s, 2H, C_2, C_6-Ph'-H), 7.51 (d, J = 11.9 Hz, 1H, C_5-thiophene-H), 7.50–7.37 (m, 2H, C_2, C_6-Ph''-H), 7.23–7.18 (m, 2H C_3, C_5-Ph''-H), 6.53 (d, J = 16.7 Hz, 1H, = CHCN), 2.99 (d, J = 7.1 Hz, 4H), 2.57–2.45 (m, 4H), 2.14 (s, 6H), 1.34 (s, 1H, NH). ^{13}C NMR (100 MHz, DMSO-d_6) δ 172.11, 162.69, 156.91, 152.41, 150.62, 146.32, 132.98, 131.95, 131.83, 128.77, 116.12, 96.77, 49.12, 45.11, 29.06, 16.55. ESI-MS: *m/z* 483.5 $[M + 1]^+$. $C_{27}H_{26}N_6OS$ (482.19).

4.1.8. (E)-3-(4-((2-((4-(3-aminopiperidin-1-yl)phenyl)amino)thieno[3,2-d]pyrimidin-4-yl)oxy)-3,5-dimethylphenyl)acrylonitrile (21a)

Recrystallized from EA/PE as a brown solid, 64% yield, mp: 166–167 °C. ^{1}H NMR (400 MHz, DMSO-d_6) δ 9.29 (s, 1H, NH), 7.68 (d, J = 16.6 Hz, 1H, ArCH =), 7.56 (s, 2H, C_2, C_6-Ph'-H), 7.45 (d, J = 5.3 Hz, 1H, C_6-thiophene-H), 7.34 (d, J = 5.3 Hz, 1H, C_7-thiophene-H), 6.97–6.84 (m, 2H, C_2, C_6-Ph''-H), 6.80–6.71 (m, 2H, C_3, C_5-Ph''-H), 6.30 (d, J = 16.7 Hz, 1H, = CHCN), 3.24–3.12 (m, 4H), 2.74 (d, J = 7.6 Hz, 1H), 2.12 (s, 6H), 1.69–1.55 (m, 2H), 1.50–1.45 (m, 2H), 1.33 (s, 2H, NH_2). ^{13}C NMR (100 MHz, DMSO-d_6) δ 164.97, 162.89, 159.62, 158.38, 151.33, 138.09, 137.38, 131.93, 131.55, 128.75, 128.20, 127.07, 124.31, 123.74, 120.05, 119.32, 117.31, 111.17, 96.98, 96.78, 54.55, 50.18, 47.24, 29.02, 22.57, 16.51, 16.38. ESI-MS: *m/z* 497.7 $[M + 1]^+$. $C_{28}H_{28}N_6OS$ (496.20).

4.1.9. (E)-3-(4-((2-((4-(3-aminopiperidin-1-yl)phenyl)amino)thieno[2,3-d]pyrimidin-4-yl)oxy)-3,5-dimethylphenyl)acrylonitrile (21b)

Recrystallized from EA/PE as a white solid, 64% yield, mp: 205–206 °C. ^{1}H NMR (400 MHz, DMSO-d_6) δ 9.33 (s, 1H, NH), 7.62 (d, J = 16.5 Hz, 1H, ArCH =), 7.49 (s, 2H, C_2, C_6-Ph'-H), 7.38 (d, J = 6.0 Hz, 1H, C_6-thiophene-H), 7.32 (d, J = 5.9 Hz, 1H, C_5-thiophene-H), 7.11–7.08 (m, 2H, C_2, C_6-Ph''-H), 6.52–6.48 (m, 2H, C_3, C_5-Ph''-H), 6.45 (d, J = 16.7 Hz, 1H, = CHCN), 3.30–3.21 (m, 4H), 2.71–2.65 (m, 1H), 2.45–2.43 (m, 2H), 2.22–2.16 (m, 2H), 2.14 (s, 6H), 1.26 (s, 2H, NH_2). ^{13}C NMR (100 MHz, DMSO-d_6) δ 172.13, 162.68, 156.96, 152.41, 150.58, 146.79, 132.37, 131.94, 131.82, 128.74, 120.47, 120.13, 119.39, 118.73, 116.49, 96.79, 60.23, 59.27, 49.92, 48.10, 33.88, 29.03, 24.08, 21.23, 16.56, 14.56. ESI-MS: *m/z* 497.7 $[M + 1]^+$. $C_{28}H_{28}N_6OS$ (496.20).

4.1.10. General procedure for the preparation of final compounds 16a1-2, 16b1-2, 19a1-2, 19b1-2, 22a1-2, and 22b1-2

Intermediates **15a** (or **15b**, **18a-b** and **21a-b**) were dissolved in anhydrous DCM (10 mL) in the presence of Et_3N (1.2 eq), followed by addition of the substituted sulfonyl chloride (1.2 eq) at 0 °C. The reaction mixture was stirred at room temperature for 2–5 h (monitored by TLC), and to the reaction was added 10 mL DCM. The organic phase was washed with saturated sodium chloride (3 × 5 mL), then dried over anhydrous Na_2SO_4, filtered, and purified by flash column chromatography. The product was recrystallized from ethyl acetate/petroleum ether to afford the target compounds **16a1-2**, **16b1-2**, **19a1-2**, **19b1-2**, **22a1-2**, and **22b1-2**.

4.1.11. (E)-4-(4-((4-(4-(2-cyanovinyl)-2,6-dimethylphenoxy)thieno[3,2-d]pyrimidin-2-yl)amino)benzyl)piperazine-1-sulfonamide (16a1)

Recrystallized from EA/PE as a yellow solid, 44% yield, mp:

160–162 °C. ^{1}H NMR (400 MHz, DMSO-d_6) δ 9.52 (s, 1H, NH), 8.43 (d, J = 16.7 Hz, 1H, ArCH =), 7.95 (d, J = 4.7 Hz, 1H, C_6-thiophene-H), 7.73 (s, 2H, C_2, C_6-Ph'-H), 7.59–7.52 (m, 2H, C_2, C_6-Ph''-H), 7.37 (s, 2H, SO_2NH_2) 7.20 (d, J = 5.2 Hz, 1H, C_7-thiophene-H), 7.03–6.96 (m, 2H, C_3, C_5-Ph''-H), 6.40 (d, J = 16.7 Hz, 1H, =CHCN), 3.50 (s, 2H, CH_2), 3.44–3.41 (m, 4H), 2.45–2.34 (m, 4H), 2.12 (s, 6H). ESI-MS: m/z 576.7 $[M + 1]^+$. $C_{28}H_{29}N_7O_3S_2$(575.18).

4.1.12. (E)-3-(3,5-dimethyl-4-((2-((4-((4-(methylsulfonyl) piperazin-1-yl)methyl)phenyl)amino)thieno[3,2-d]pyrimidin-4-yl) oxy)phenyl)acrylonitrile (16a2)

Recrystallized from EA/PE as a white solid, 52% yield, mp: 120–121 °C. ^{1}H NMR (400 MHz, DMSO-d_6) δ 9.50 (s, 1H, NH), 7.69 (d, J = 17.0 Hz, 1H, ArCH =), 8.32 (d, J = 4.7 Hz, 1H, C_6-thiophene-H), 7.57 (s, 2H, C_2, C_6-Ph'-H), 7.49–7.42 (m, 2H, C_2, C_6-Ph''-H), 7.39 (d, J = 5.2 Hz, 1H, C_7-thiophene-H), 7.03–6.96 (m, 2H, C_3, C_5-Ph''-H), 6.50 (d, J = 16.7 Hz, 1H, =CHCN), 3.39 (s, 2H, N–CH_2), 3.10 (s, 3H, SO_2CH_3), 2.92–2.85 (m, 4H), 2.53–2.48 (m, 4H), 2.12 (s, 6H). ^{13}C NMR (100 MHz, DMSO-d_6) δ 165.32, 162.98, 158.21, 150.51, 139.97, 137.59, 132.17, 131.91, 129.70, 129.27, 128.75, 123.81, 118.62, 107.12, 97.00, 61.63, 52.14, 45.93, 34.11, 29.00, 16.52. ESI-MS: m/z 575.5 $[M + 1]^+$. $C_{29}H_{30}N_6O_3S_2$(574.18).

4.1.13. (E)-4-(4-((4-(4-(2-cyanovinyl)-2,6-dimethylphenoxy)thieno [2,3-d]pyrimidin-2-yl)amino)benzyl)piperazine-1-sulfonamide (16b1)

Recrystallized from EA/PE as a yellow solid, 43% yield, mp: 142–144 °C. ^{1}H NMR (400 MHz, DMSO-d_6) δ 9.65 (s, 1H, NH), 7.70 (d, J = 16.7 Hz, 1H, ArCH =), 7.57 (s, 2H, C_2, C_6-Ph'-H), 7.49 (d, J = 5.8 Hz, 1H, C_6-thiophene-H), 7.46 (d, J = 5.9 Hz, 1H, C_5-thiophene-H), 7.43 (s, 2H, SO_2NH_2), 7.41 (d, J = 6.4 Hz, 2H, C_2, C_6-Ph''-H), 7.04–6.90 (m, 2H, C_3, C_5-Ph''-H), 6.50 (d, J = 16.7 Hz, 1H, =CHCN), 3.56 (s, N–CH_2), 2.42–2.33 (m, 4H), 2.30–2.25 (m, 4H), 2.12 (s, 6H). ESI-MS: m/z 576.7 $[M + 1]^+$. $C_{28}H_{29}N_7O_3S_2$ (575.18).

4.1.14. (E)-3-(3,5-dimethyl-4-((2-((4-((4-(methylsulfonyl) piperazin-1-yl)methyl)phenyl)amino)thieno[2,3-d]pyrimidin-4-yl) oxy)phenyl)acrylonitrile (16b2)

Recrystallized from EA/PE as a white solid, 54% yield, mp: 149–151 °C. ^{1}H NMR (400 MHz, DMSO-d_6) δ 9.57 (s, 1H, NH), 7.62 (d, J = 16.6 Hz, 1H, ArCH =), 7.50 (s, 2H, C_2, C_6-Ph'-H), 7.41 (d, J = 8.3 Hz, 2H, C_2, C_6-Ph''-H), 7.34 (d, J = 4.4 Hz, 1H, C_6-thiophene-H), 7.28 (d, J = 8.3 Hz, 2H, C_3, C_5-Ph''-H), 6.89 (d, J = 4.5 Hz, 1H, C_5-thiophene-H), 6.43 (d, J = 16.7 Hz, 1H, =CHCN), 3.05–3.02 (m, 4H), 2.81 (s, 3H, SO_2CH_3), 2.35–2.32 (m, 4H), 2.15 (s, 6H), 1.87 (s, 2H, N–CH_2). ^{13}C NMR (100 MHz, DMSO-d_6) δ 162.66, 156.96, 150.53, 131.93, 131.82, 131.37, 128.73, 128.20, 127.41, 119.36, 118.74, 116.71, 96.82, 56.71, 50.64, 49.78, 49.68, 31.48, 29.03, 23.81, 16.58, 16.48. ESI-MS: m/z 575.7 $[M + 1]^+$. $C_{29}H_{30}N_6O_3S_2$ (574.18).

4.1.15. (E)-3-(3,5-dimethyl-4-((2-((4-(piperazin-1-yl)phenyl) amino)thieno[3,2-d]pyrimidin-4-yl)oxy)phenyl)acrylonitrile (19a1)

Recrystallized from EA/PE as a white solid, 65% yield, mp: 157–159 °C. ^{1}H NMR (400 MHz, DMSO-d_6) δ 9.28 (s, 1H, NH), 8.30 (d, J = 5.4 Hz, 1H, C_6-thiophene-H), 7.70 (d, J = 16.7 Hz, 1H, ArCH =), 7.57 (s, 2H, C_2, C_6-Ph' –H), 7.34 (d, J = 5.3 Hz, 1H, C_7-thiophene-H), 7.32–7.25 (m, 2H, C_2, C_6-Ph''-H), 6.70 (m, 2H, C_3, C_5-Ph''-H), 6.53 (d, J = 16.7 Hz, 1H, =CHCN), 2.70–2.65 (m, 4H), 2.36–2.32 (m, 4H), 2.12 (s, 6H), 1.24 (s, 1H, NH). ESI-MS: m/z 483.5 $[M + 1]^+$. $C_{27}H_{26}N_6OS$ (482.19).

4.1.16. (E)-3-(3,5-dimethyl-4-((2-((4-(4-(methylsulfonyl)piperazin-1-yl)phenyl)amino)thieno[3,2-d]pyrimidin-4-yl)oxy)phenyl) acrylonitrile (19a2)

Recrystallized from EA/PE as a yellow solid, 51% yield, mp: 201–202 °C. ^{1}H NMR (400 MHz, DMSO-d_6) δ 9.23 (s, 1H, NH), 8.22 (d, J = 5.2 Hz, 1H, C_6-thiophene-H), 7.63 (d, J = 16.7 Hz, 1H, ArCH =), 7.49 (s, 2H, C_2, C_6-Ph'-H), 7.27 (d, J = 5.3 Hz, 1H, C_7-thiophene-H), 7.25 (d, J = 8.2 Hz, 2H, C_2, C_6-Ph''-H), 6.61 (d, J = 8.1 Hz, 2H, C_3, C_5-Ph''-H), 6.45 (d, J = 16.7 Hz, 1H, =CHCN), 3.19–3.16 (m, 4H), 3.05–3.00 (m, 4H), 2.86 (s, 3H, SO_2CH_3), 2.14 (s, 6H). ^{13}C NMR (100 MHz, DMSO-d_6) δ 165.47, 162.96, 158.36, 152.07, 150.55, 145.51, 137.35, 133.95, 132.12, 131.93, 128.77, 123.75, 119.97, 119.35, 116.85, 96.95, 49.39, 45.88, 34.27, 31.43, 22.53, 16.50, 14.43. ESI-MS: m/z 561.7 $[M + 1]^+$. $C_{28}H_{28}N_6O_3S_2$ (560.17).

4.1.17. (E)-4-(4-((4-(4-(2-cyanovinyl)-2,6-dimethylphenoxy)thieno [2,3-d]pyrimidin-2-yl)amino)phenyl)piperazine-1-sulfonamide (19b1)

Recrystallized from EA/PE as a white solid, 42% yield, mp: 161–163 °C. ^{1}H NMR (400 MHz, DMSO-d_6) δ 9.52 (s, 1H, NH), 7.75 (d, J = 16.6 Hz, 1H, ArCH =), 7.60 (s, 2H, C_2, C_6-Ph'-H), 7.51 (d, J = 6.0 Hz, 1H, C_6-thiophene-H), 7.46 (d, J = 6.0 Hz, 1H, C_5-thiophene-H), 7.39 (s, 2H, SO_2NH_2), 7.32–7.18 (m, 2H, C_2, C_6-Ph''-H), 6.82–6.64 (m, 2H, C_3, C_5-Ph''-H), 6.57 (d, J = 16.7 Hz, 1H, =CHCN), 3.88–3.62 (m, 4H), 3.16–3.07 (m, 4H), 2.15 (s, 6H). ESI-MS: m/z 562.5 $[M + 1]^+$. $C_{27}H_{27}N_7O_3S_2$ (561.16). (E)-3-(3,5-dimethyl-4-((2-((4-(4-(methylsulfonyl)piperazin-1-yl)phenyl)amino)thieno[2,3-d]pyrimidin-4-yl)oxy)phenyl)acrylonitrile (19b2).

Recrystallized from EA/PE as a white solid, 56% yield, mp: 218–220 °C. ^{1}H NMR (400 MHz, DMSO-d_6) δ 9.47 (s, 1H, NH), 7.71 (d, J = 16.7 Hz, 1H, ArCH =), 7.56 (s, 2H, C_2, C_6-Ph'-H), 7.47 (d, J = 5.9 Hz, 1H, C_6-thiophene-H), 7.42 (d, J = 5.9 Hz, 1H, C_5-thiophene-H), 7.25–7.20 (m, 2H, C_2, C_6-Ph''-H), 6.74–6.68 (m, 2H, C_3, C_5-Ph''-H), 6.52 (d, J = 16.7 Hz, 1H, =CHCN), 3.36–3.25 (m, 4H), 3.15–3.09 (m, 4H), 2.93 (s, 3H, SO_2CH_3), 2.11 (s, 6H). ^{13}C NMR (100 MHz, DMSO-d_6) δ 172.08, 162.69, 156.89, 152.38, 150.62, 133.44, 131.96, 131.84, 129.70, 128.76, 122.61, 120.66, 120.07, 118.73, 116.75, 99.99, 96.81, 49.28, 48.54, 45.85, 45.68, 43.31, 34.27, 16.68, 16.55.ESI-MS: m/z 561.5 $[M + 1]^+$. $C_{28}H_{28}N_6O_3S_2$ (560.17).

4.1.18. (E)-N-(1-(4-((4-(4-(2-cyanovinyl)-2,6-dimethylphenoxy) thieno[3,2-d]pyrimidin-2-yl)amino)phenyl)piperidin-3-yl) sulfonamide (22a1)

Recrystallized from EA/PE as a white solid, 41% yield, mp: 147–148 °C. ^{1}H NMR (400 MHz, DMSO-d_6) δ 9.42 (s, 1H, NH), 7.45 (d, J = 16.7 Hz, 1H, ArCH =), 7.44 (d, J = 5.4 Hz, 1H, NH), 7.35 (d, J = 8.6 Hz, 2H, C_2, C_6-Ph''-H), 7.22 (s, 2H, C_2, C_6-Ph'-H), 6.87 (d, J = 8.9 Hz, 1H, C_6-thiophene-H), 6.85 (s, 2H, SO_2NH_2), 6.75 (d, J = 9.1 Hz, 1H, C_7-thiophene-H), 6.51 (d, J = 8.7 Hz, 2H, C_3, C_5-Ph''-H), 6.29 (d, J = 16.7 Hz, 1H, =CHCN), 3.67–3.49 (m, 2H), 2.72–2.56 (m, 2H), 2.19–2.15 (m, 1H), 2.14 (s, 6H), 1.82–1.72 (m, 2H), 1.64–1.49 (m, 2H). ^{13}C NMR (100 MHz, DMSO-d_6) δ 164.97, 162.87, 159.64, 151.33, 150.26, 148.37, 138.01, 133.87, 131.91, 131.66, 131.55, 128.20, 127.22, 124.32, 119.28, 116.16, 111.10, 96.75, 53.07, 49.30, 46.72, 29.67, 23.59, 16.51, 16.37. ESI-MS: m/z 576.5 $[M + 1]^+$. $C_{28}H_{29}N_7O_3S_2$(575.18).

4.1.19. (E)-N-(1-(4-((4-(4-(2-cyanovinyl)-2,6-dimethylphenoxy) thieno[3,2-d]pyrimidin-2-yl)amino)phenyl)piperidin-3-yl) methanesulfonamide (22a2)

Recrystallized from EA/PE as a white solid, 56% yield, mp: 122–124 °C. ^{1}H NMR (400 MHz, DMSO-d_6) δ 9.18 (s, 1H, NH), 8.21 (d, J = 5.3 Hz, 1H, NH), 7.60 (d, J = 16.7 Hz, 1H, ArCH =), 7.49 (s, 2H, C_2, C_6-Ph'-H), 7.27 (d, J = 7.1 Hz, 1H, C_6-thiophene-H), 7.26–7.11 (m, 2H, C_2, C_6-Ph''-H), 7.10 (d, J = 7.1 Hz, 1H, C_7-thiophene-H), 6.70–6.53 (m, 2H, C_3, C_5-Ph''-H), 6.43 (d, J = 16.7 Hz, 1H, =CHCN), 3.45–3.42 (m, 1H), 2.90 (s, 3H, SO_2CH_3), 2.47–2.37 (m, 4H), 2.15 (s, 6H), 1.90–1.81 (m, 2H), 1.74–1.66 (m, 2H). ^{13}C NMR (100 MHz, DMSO-d_6) δ 165.46, 162.92, 158.43, 152.03, 150.48, 146.01, 137.29, 133.24,

132.09, 131.91, 128.75, 123.76, 120.13, 119.34, 116.81, 96.96, 56.82, 49.81, 31.48, 23.84, 16.52. ESI-MS: *m/z* 575.5 $[M + 1]^+$. $C_{29}H_{30}N_6O_3S_2$(574.18).

4.1.20. (E)-N-(1-(4-((4-(4-(2-cyanovinyl)-2,6-dimethylphenoxy) thieno[2,3-d]pyrimidin-2-yl)amino)phenyl)piperidin-3-yl) sulfonamide (22b1)

Recrystallized from EA/PE as a yellow solid, 45% yield, mp: 200–202 °C. ^{1}H NMR (400 MHz, DMSO-d_6) δ 9.30 (s, 1H, NH), 7.61 (d, J = 16.7 Hz, 1H, ArCH =), 7.48 (s, 2H, C_2, C_6-Ph'-H), 7.43 (d, J = 7.7 Hz, 1H, NH), 7.38 (d, J = 5.9 Hz, 1H, C_6-thiophene-H), 7.33 (d, J = 6.0 Hz, 1H, C_5-thiophene-H), 7.28 (s, 2H, SO_2NH_2), 7.18–7.07 (m, 2H, C_2, C_6-Ph''-H), 6.59–6.52 (m, 2H, C_3, C_5-Ph''-H), 6.43 (d, J = 16.7 Hz, 1H, = CHCN), 3.46–3.40 (m, 4H), 3.37–3.31 (m, 1H), 2.14 (s, 6H), 1.94–1.84 (m, 2H), 1.71–1.64 (m, 2H). ESI-MS: *m/z* 576.7 $[M + 1]^+$. $C_{28}H_{29}N_7O_3S_2$ (575.18).

4.1.21. (E)-N-(1-(4-((4-(4-(2-cyanovinyl)-2,6-dimethylphenoxy) thieno[2,3-d]pyrimidin-2-yl)amino)phenyl)piperidin-3-yl) methanesulfonamide (22b2)

Recrystallized from EA/PE as a yellow solid, 57% yield, mp: 144–146 °C. ^{1}H NMR (400 MHz, DMSO-d_6) δ 9.34 (s, 1H, NH), 7.67 (d, J = 15.8 Hz, 1H, ArCH =), 7.48 (s, 2H, C_2, C_6-Ph'-H), 7.45 (dd, J = 6.0, 2.1 Hz, 2H, C_2, C_6-Ph''-H), 7.38 (d, J = 5.9 Hz, 1H, C_6-thiophene-H), 7.33 (d, J = 5.9 Hz, 1H, C_5-thiophene-H), 7.13–7.08 (m, 2H, C_3, C_5-Ph''-H), 7.01 (s, 1H, NH), 6.74 (d, J = 15.8 Hz, 1H, = CHCN), 2.94–2.90 (m, 2H), 2.57–2.49 (m, 2H), 2.49–2.45 (m, 1H), 2.43 (s, 3H, SO_2CH_3), 2.14 (s, 6H), 1.92–1.85 (m, 2H), 1.28–1.24 (m, 2H). ^{13}C NMR (100 MHz, DMSO-d_6) δ 162.66, 156.96, 150.53, 131.82, 131.37, 128.73, 128.20, 127.41, 118.74, 116.71, 96.82, 56.71, 50.64, 49.78, 49.68, 29.03, 23.81, 16.58, 16.48. ESI-MS: *m/z* 575.7 $[M + 1]^+$. $C_{29}H_{30}N_6O_3S_2$ (574.18).

4.2. In vitro anti-HIV-1 assay

Using MTT method, the anti-HIV-1 activity assay was performed in MT-4 cells. Compounds stock solutions (10 × final concentration) were added in 25 μL volumes to two series of triplicate wells to allow simultaneous evaluation of their effects on mock- and HIV-infected cells [26,27]. Serial 5-fold dilutions of compounds were made directly in flat-bottomed 96-well microtiter trays using a Biomek 3000 robot (Beckman instruments, Fullerton, CA). Untreated HIV- and mock-infected cell samples were included as controls. HIV stock (50 μL) at 100–300 $CCID_{50}$ (50% cell culture infectious doses) or culture medium was added to either the infected or mock-infected cell wells of the microtiter tray. Mock-infected cells were used to evaluate the effects of test compound on uninfected cells to assess the cytotoxicity of the compounds. Exponentially growing MT-4 cells were centrifuged for 5 min at 220 g and the supernatant was discarded. The MT-4 cells were resuspended at 6 × 10^5 cells/mL and 50 μL volumes were transferred to the microtiter tray wells. Five days after infection, the viability of mock-and HIV-infected cells was examined spectrophotometrically using the MTT assay. The absorbances were read in an eight-channel computer-controlled photometer (Infinite M1000, Tecan), at two wavelengths (540 and 690 nm). All data were calculated using the median absorbance value of three wells. The 50% cytotoxic concentration (CC_{50}) was defined as the concentration of the compounds that reduced the absorbance (OD_{540}) of the mock-infected control sample by 50%. The concentration achieving 50% protection against the cytopathic effect of the virus in infected cells was defined as the 50% effective concentration (EC_{50}).

4.3. HIV-1 RT inhibition assays

The HIV-1 reverse transcriptase (RT) assay kit (Roche) was used to perform the RT inhibition assay. All the reagents for performing the RT reaction were from the kit and the particular ELISA procedures were carried out following the description in the kit protocol [28]. Firstly, the reaction mixture containing the template/primer complex, viral nucleotides (dNTPs) and RT in the incubation buffer with or without inhibitors was incubated for 1 h at 37 °C. After that, the reaction mixture was transferred to a streptavidin-coated microtiter plate and incubated for another 1 h at 37 °C to ensure that the retranscriptional cDNA chain that contained biotin-labeled dNTPs was bound to streptavidin. Then un-bound dNTPs were removed using washing buffer and anti-DIG-POD working solution was added. After incubation for another 1 h at 37 °C, the DIG-labeled dNTPs incorporated into cDNA were bound to the anti-DIG-POD antibody. The unbound anti-DIG-PODs were removed and the peroxide substrate (ABST) solution was added to the MTPs. A colored reaction proceeds during the cleavage of the substrate catalyzed by POD. The absorbance of the sample was determined at OD405 nm using a microtiter plate ELISA reader. The percentage inhibitory activity of RT inhibitors was calculated using the formula as given below:

Inhibition (%) = (OD value with RT but without inhibitors-OD value with RT and inhibitors)/(OD value with RT and inhibitors-OD value without RT and inhibitors).

4.4. Water solubility measurement

Compound **16a1** or **16b1** (0.1, 1, 10 mg) was dissolved in deionized water (pH = 2.0, 7.0, and 7.4) until the solution was clear. The assays were measured at least in duplicate [14].

4.5. Molecular simulation studies

The molecular modelling study was performed by Sybyl-X 2.0 software. All the molecules were built using standard bond lengths and angles from Sybyl-X 2.0/Base Builder and optimized using the Tripos force field for 1000 generations, until the minimized conformers of the ligand were the same. The flexible docking method (Surflex-Dock) docks the ligand automatically into the ligand-binding site of the receptor with a protocol-based approach and an empirically derived scoring function. The protocol is a computational representation of a putative ligand that binds to the intended binding site and is a unique and essential element of the docking algorithm. The scoring function in Surflex-Dock, containing hydrophobic, polar, repulsive, entropic, and solvation terms, was trained to estimate the dissociation constant (Kd). The protein was prepared by removing the ligand and other unnecessary small molecules from the cocrystal structures (PDB code: 6c0n, 6c0r)), polar hydrogen atoms and charges were added to the protein before docking. During the docking procedure, all of the single bonds in residue side-chains inside the defined RT binding pocket were regarded as rotatable or flexible, and the ligand was allowed to rotate at all single bonds and to move flexibly within the tentative binding pocket. The atomic charges were recalculated using the Kollman all-atom approach for the protein and the Gasteiger-Hückel approach for the ligand. The binding interaction energy was calculated, including van der Waals, electrostatic, and torsional energy terms defined in the Tripos force field. The structure optimization was performed for 10,000 generations using a genetic algorithm, and the 20-best-scoring ligand-protein complexes were kept for further analysis. The -log $(Kd)^2$ values of the 20-best-scoring complexes, representing the binding affinities of ligand with RT, encompassed a wide range of functional classes

(10^{-2}-10^{-9}). The highest-scoring 3D structural model of ligand-bound RT was chosen to define the binding interaction [25].

Author contributions

All authors contributed to writing the manuscript. All authors have given approval to the final version of the manuscript.

Notes

The authors declare no competing financial interest.

Declaration of competing interest

The authors declare that they have no known competing financial interests or personal relationships that could have appeared to influence the work reported in this paper.

Acknowledgments

We acknowledge financial support from the National Natural Science Foundation of China (NSFC Nos. 81973181, 81903453), Shandong Provincial Key research and development project (Nos. 2019JZZY021011), Natural Science Foundation of Jiangsu Province (BK2019041035), Shandong Provincial Natural Science Foundation (ZR2019BH011, ZR2020YQ61), China Postdoctoral Science Foundation (2019T120596), Young Scholars Program of Shandong University (YSPSDU No. 2016WLJH32), National Science and Technology Major Projects for "Major New Drugs Innovation and Development" (2019ZX09301126), the Taishan Scholar Program at Shandong Province. The technical assistance of Mr. Kris Uyttersprot and Mrs. Kristien Erven, for the HIV experiments is gratefully acknowledged.

Appendix A. Supplementary data

Supplementary data to this article can be found online at https://doi.org/10.1016/j.ejmech.2021.113204.

References

[1] D.M. Margolis, N.M. Archin, M.S. Cohen, J.J. Eron, G. Ferrari, V. Garcia, C.L. Gay, N. Goonetilleke, S.B. Joseph, R. Swanstrom, A.-M.W. Turner, A. Wahl, Curing HIV: seeking to target and clear persistent infection, Cell 181 (2020) 189–206.
[2] R.J. Shattock, M. Warren, S. McCormack, C.A. Hankins, Turning the tide against HIV, Science 333 (2011) 42–43.
[3] G. Bec, B. Meyer, M.-M. Gerard, J. Steger, K. Fauster, P. Wolff, D. Burnouf, R. Micura, P. Dumas, E. Ennifar, Thermodynamics of HIV-1 reverse transcriptase in action elucidates the mechanism of action of non-nucleoside inhibitors, J. Am. Chem. Soc. 135 (2013) 9743–9752.
[4] C. Zhuang, C. Pannecouque, E. De Clercq, F. Chen, Development of non-nucleoside reverse transcriptase inhibitors (NNRTIs): our past twenty years, Acta Pharm. Sin. B. 10 (2020) 961–978.
[5] P. Zhan, X. Chen, D. Li, Z. Fang, E. De Clercq, X. Liu, HIV-1 NNRTIs: structural diversity, pharmacophore similarity, and impliations for drug design, Med. Res. Rev. 33 (2013) E1–E72.
[6] L. Wang, S.G. Sarafianos, Z. Wang, Cutting into the substrate dominance: pharmacophore and structure-based approaches toward inhibiting human immunodeficiency virus reverse transcriptase-associated ribonuclease H, Accounts Chem. Res. 53 (2020) 218–230.
[7] V. Namasivayam, M. Vanangamudi, V.G. Kramer, S. Kurup, P. Zhan, X. Liu, J. Kongsted, S.N. Byrareddy, The journey of HIV-1 non-nucleoside reverse transcriptase inhibitors (NNRTIs) from lab to clinic, J. Med. Chem. 62 (2019) 4851–4883.
[8] P. Zhan, C. Pannecouque, E. De Clercq, X. Liu, Anti-HIV drug discovery and development: current innovations and future trends, J. Med. Chem. 59 (2016) 2849–2878.
[9] D.A. Lehman, D.C. Wamalwa, C.O. McCoy, F.A. Matsen, A. Langat, B.H. Chohan, S. Benki-Nugent, R. Custers-Allen, F.D. Bushman, G.C. John-Stewart, J. Overbaugh, Low-frequency nevirapine resistance at multiple sites may predict treatment failure in infants on nevirapine-based treatment, Jaids-J. Acq. Imm. Def. 60 (2012) 225–233.
[10] C. Beyrer, A. Pozniak, HIV drug resistance - an emerging threat to epidemic control, N. Engl. J. Med. 377 (2017) 1605–1607.
[11] H. Xu, E.L. Asahchop, M. Oliveira, P.K. Quashie, Y. Quan, B.G. Brenner, M.A. Wainberg, Compensation by the E138K mutation in HIV-1 reverse transcriptase for deficits in viral replication capacity and enzyme processivity associated with the M184I/V mutations, J. Virol. 85 (2011) 11300–11308.
[12] D. Kang, Z. Fang, Z. Li, B. Huang, H. Zhang, X. Lu, H. Xu, Z. Zhou, X. Ding, D. Daelemans, E. De Clercq, C. Pannecouque, P. Zhan, X. Liu, Design, synthesis, and evaluation of thiophene 3,2-d pyrimidine derivatives as HIV-1 non-nucleoside reverse transcriptase inhibitors with significantly improved drug resistance profiles, J. Med. Chem. 59 (2016) 7991–8007.
[13] M. Feng, D. Wang, J.A. Grobler, D.J. Hazuda, M.D. Miller, M.-T. Lai, Vitro resistance selection with doravirine (MK-1439), a novel nonnucleoside reverse transcriptase inhibitor with distinct mutation development pathways, Antimicrob. Agents Chemother. 59 (2015) 590–598.
[14] B. Huang, W. Chen, T. Zhao, Z. Li, X. Jiang, T. Ginex, D. Vilchez, F.J. Luque, D. Kang, P. Gao, J. Zhang, Y. Tian, D. Daelemans, E. De Clercq, C. Pannecouque, P. Zhan, X. Liu, Exploiting the tolerant region I of the non-nucleoside reverse transcriptase inhibitor (NNRTI) binding pocket: discovery of potent diarylpyrimidine-typed HIV-1 NNRTIs against wild-type and E138K mutant virus with significantly improved water solubility and favorable safety profiles, J. Med. Chem. 62 (2019) 2083–2098.
[15] D. Kang, F.X. Ruiz, D. Feng, A. Pilch, T. Zhao, F. Wei, Z. Wang, Y. Sun, Z. Fang, E. De Clercq, C. Pannecouque, E. Arnold, X. Liu, P. Zhan, Discovery and characterization of fluorine-substituted diarylpyrimidine derivatives as novel HIV-1 NNRTIs with highly improved resistance profiles and low activity for the hERG ion channel, J. Med. Chem. 63 (2020) 1298–1312.
[16] X. Zuo, Z. Huo, D. Kang, G. Wu, Z. Zhou, X. Liu, P. Zhan, Current insights into anti-HIV drug discovery and development: a review of recent patent literature (2014-2017), Expert Opin. Ther. Pat. 28 (2018) 299–316.
[17] Y. Sang, S. Han, C. Pannecouque, E. De Clercq, C. Zhuang, F. Che, Ligand-based design of nondimethylphenyl-diarylpyrimidines with improved metabolic stability, safety, and oral pharmacokinetic profiles, J. Med. Chem. 62 (2019) 11430–11436.
[18] D. Kang, H. Zhang, Z. Wang, T. Zhao, T. Ginex, F.J. Luque, Y. Yang, G. Wu, D. Feng, F. Wei, J. Zhang, E. De Clercq, C. Pannecouque, C.H. Chen, K.-H. Lee, N.A. Murugan, T.A. Steitz, P. Zhan, X. Liu, Identification of dihydrofuro 3,4-d pyrimidine derivatives as novel HIV-1 non-nucleoside reverse transcriptase inhibitors with promising antiviral activities and desirable physicochemical properties, J. Med. Chem. 62 (2019) 1484–1501.
[19] D. Kang, T. Zhao, Z. Wang, D. Feng, H. Zhang, B. Huang, G. Wu, F. Wei, Z. Zhou, L. Jing, X. Zuo, Y. Tian, V. Poongavanam, J. Kongsted, E. De Clercq, C. Pannecouque, P. Zhan, X. Liu, Discovery of piperidine-substituted thiazolo 5,4-d pyrimidine derivatives as potent and orally bioavailable HIV-1 non-nucleoside reverse transcriptase inhibitors, Commun. Chem. 2 (2019) 74.
[20] D. Kang, D. Feng, L. Jing, Y. Sun, F. Wei, X. Jiang, G. Wu, E. De Clercq, C. Pannecouque, P. Zhan, X. Liu, In situ click chemistry-based rapid discovery of novel HIV-1 NNRTIs by exploiting the hydrophobic channel and tolerant regions of NNIBP, Eur. J. Med. Chem. 193 (2020), 112237.
[21] D. Kang, Y. Sun, N.A. Murugan, D. Feng, F. Wei, J. Li, X. Jiang, E. De Clercq, C. Pannecouque, P. Zhan, X. Liu, Structure-activity relationship exploration of NNIBP tolerant region I leads to potent HIV-1 NNRTIs, ACS Infect. Dis. 6 (2020) 2225–2234.
[22] D. Kang, D. Feng, Y. Sun, Z. Fang, F. Wei, E. De Clercq, C. Pannecouque, X. Liu, P. Zhan, Structure-based bioisosterism yields HIV-1 NNRTIs with improved drug-resistance profiles and favorable pharmacokinetic properties, J. Med. Chem. 63 (2020) 4837–4848.
[23] D. Kang, D. Feng, T. Ginex, J. Zou, F. Wei, T. Zhao, B. Huang, Y. Sun, S. Desta, E. De Clercq, C. Pannecouque, P. Zhan, X. Liu, Exploring the hydrophobic channel of NNIBP leads to the discovery of novel piperidine-substituted thiophene[3,2-d]pyrimidine derivatives as potent HIV-1 NNRTIs, Acta Pharm. Sin. B. 10 (2020) 878–894.
[24] D. Kang, Z. Fang, B. Huang, X. Lu, H. Zhang, H. Xu, Z. Huo, Z. Zhou, Z. Yu, Q. Meng, G. Wu, X. Ding, Y. Tian, D. Daelemans, E. De Clercq, C. Pannecouque, P. Zhan, X. Liu, Structure-based optimization of thiophene 3,2-d pyrimidine derivatives as potent HIV-1 non-nucleoside reverse transcriptase inhibitors with improved potency against resistance-associated variants, J. Med. Chem. 60 (2017) 4424–4443.
[25] Y. Yang, D. Kang, L.A. Nguyen, Z.B. Smithline, C. Pannecouque, P. Zhan, X. Liu, T.A. Steitz, Structural basis for potent and broad inhibition of HIV-1 RT by thiophene 3,2-d pyrimidine non-nucleoside inhibitors, elife 7 (2018), e36340 pii.
[26] C. Pannecouque, D. Daelemans, E. De Clercq, Tetrazolium-based colorimetric assay for the detection of HIV replication inhibitors: revisited 20 years later, Nat. Protoc. 3 (2008) 427–434.
[27] A. Hombrouck, A. Voet, B. Van Remoortel, C. Desadeleer, M. De Maeyer, Z. Debyser, M. Witvrouw, Mutations in human immunodeficiency virus type 1 integrase confer resistance to the naphthyridine L-870,810 and cross-resistance to the clinical trial drug GS-9137, Antimicrob. Agents, Chemother 52 (2008) 2069–2078.
[28] K. Suzuki, B.P. Craddock, N. Okamoto, T. Kano, R.T. Steigbigel, Poly A-linked colorimetric microtiter plate assay for HIV reverse transcriptase, J. Virol. Methods 44 (1993) 189–198.